

Probing the Binding Mechanism of Mnk Inhibitors by Docking and Molecular Dynamics Simulations

Srinivasaraghavan Kannan,^{*,†,‡} Anders Poulsen,[‡] Hai Yan Yang,[‡] Melvyn Ho,[‡] Shi Hua Ang,[‡] Tan Sum Wai Eldwin,[‡] Duraiswamy Athisayamani Jeyaraj,[‡] Lohitha Rao Chennamaneni,[§] Boping Liu,[‡] Jeffrey Hill,[‡] Chandra S. Verma,^{*,†,||,⊥} and Kassoum Nacro[‡]

[†]Bioinformatics Institute (A*STAR), 30 Biopolis Street, #07-01 Matrix, Singapore 138671

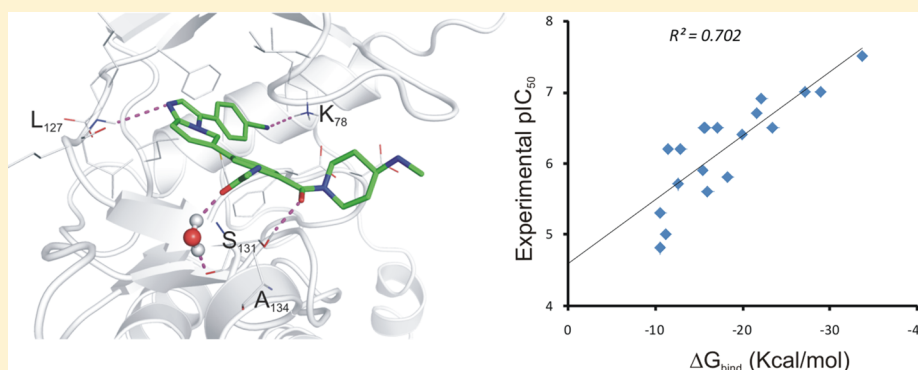
[‡]Experimental Therapeutics Centre (A*STAR), 31 Biopolis Street, #03-01 Nanos, Singapore 138669

[§]Institute of Chemical and Engineering Sciences (ICES), A*STAR, 11 Biopolis Street, #03-08 Helios, Singapore 138667

^{||}School of Biological Sciences, Nanyang Technological University, 60 Nanyang Drive, Singapore 637551

[⊥]Department of Biological Sciences, National University of Singapore, 14 Science Drive 4, Singapore 117543

S Supporting Information



ABSTRACT: Mitogen-activated protein kinases-interacting kinase 1 and 2 (Mnk1/2) activate the oncogene eukaryotic initiation factor 4E (eIF4E) by phosphorylation. High level of phosphorylated eIF4E is associated with various types of cancers. Inhibition of Mnk prevents eIF4E phosphorylation, making them potential therapeutic targets for cancer. Recently, we have designed and synthesized a series of novel imidazopyridine and imidazopyrazine derivatives that inhibit Mnk1/2 kinases with a potency in the nanomolar to micromolar range. In the current work we model the inhibition of Mnk kinase activity by these inhibitors using various computational approaches. Combining homology modeling, docking, molecular dynamics simulations, and free energy calculations, we find that all compounds bind similarly to the active sites of both kinases with their imidazopyridine and imidazopyrazine cores anchored to the hinge regions of the kinases through hydrogen bonds. In addition, hydrogen bond interactions between the inhibitors and the catalytic Lys78 (Mnk1), Lys113 (Mnk2) and Ser131 (Mnk1), Ser166 (Mnk2) appear to be important for the potency and stability of the bound conformations of the inhibitors. The computed binding free energies (ΔG_{pred}) of these inhibitors are in accord with experimental bioactivity data (pIC_{50}) with correlation coefficients (r^2) of 0.70 and 0.68 for Mnk1 and Mnk2 respectively. van der Waals energies and entropic effects appear to dominate the binding free energy (ΔG_{pred}) for each Mnk–inhibitor complex studied. The models suggest that the activities of these small molecule inhibitors arise from interactions with multiple residues in the active sites, particularly with the hydrophobic residues.

Deregulation of protein synthesis is a common event in human cancers. Eukaryotic initiation factor 4E (eIF4E), a general translation initiation factor, is a key player in translational control. It has the potential to enhance the translation of mRNAs that leads to production of malignancy-associated proteins.^{1–4} Translation of these malignancy-associated mRNAs is suppressed under normal cellular conditions as the availability of active eIF4E is limited; however, their levels can increase when eIF4E is overexpressed or hyperactivated.^{4–6} Elevated expression levels of eIF4E have been found in many types of tumors including cancers of the

colon, breast, bladder, lung, prostate, gastrointestinal tract, head, neck, Hodgkin's lymphomas, and glioblastomas.^{7–17} Recent findings suggest that eIF4E activity is a node for PI3K/Akt/mTOR and Ras/Raf/MEK/ERK pathways in mediating tumorigenic activity,¹⁸ thus rendering eIF4E as an

Special Issue: New Frontiers in Kinases

Received: October 7, 2014

Revised: November 26, 2014

Published: November 28, 2014





Figure 1. Sequence alignment of the kinase domains of human Mnk1, Mnk2, and DAPK1 proteins. The DFD motif (DFG in the DAPK1 kinase) and the Mnk specific insertions (I1, I2, and I3) are boxed with black and red colors, respectively. Identical “*”, conserved substitutions “:”, and semiconserved substitutions “.” are indicated and colored according to their amino acid properties.

important target for therapeutic development. The activity of eIF4E is regulated by posttranslational modification by mitogen activated protein (MAP) kinase-interacting kinases 1/2. Both Mnk kinases specifically phosphorylate eIF4E at the conserved Ser209 residue.^{19–23} Several studies have indicated that eIF4E phosphorylation by Mnk is critical for its oncogenic activity.^{24–33} *Drosophila* expressing a mutant eIF4E in which Ser251 (homologous to mammalian Ser209) is mutated to alanine shows reduced viability.²⁸ Mice models in which lymphomas were generated from Eμ-Myc transgenic hematopoietic stem cells transfected with mutant eIF4E (Ser209Ala) were defective in tumor development.²⁹ Mnk1/2 knockout or knock-in mice, in which Ser209 was replaced by alanine, showed no eIF4E phosphorylation and³⁰ significantly attenuated tumor growth^{25,26,31} confirming that Mnk1/2 kinase activities are essential for eIF4E phosphorylation in transformed cells. Surprisingly, mice with deletions in both Mnk1/2 develop normally,³⁰ indicating that phosphorylation of Ser209 by Mnk is essential for eIF4E's ability to promote tumorigenesis,^{25–29} while it is dispensable in normal tissue. Thus, targeting Mnk could be a potential therapeutic approach that selectively affects cancer cells.

Mnk comprise a subfamily of Ser/Thr kinases and belong to the group of Ca²⁺/calmodulin-dependent kinases (CaMK),³⁴ and like many other CaMK group members, they are not regulated by Ca²⁺/calmodulin. The catalytic domains of Mnk1/2 are highly homologous with ~80% sequence identity between them. Comparison with other protein kinases shows that Mnk possesses special insertions (I1, I2, and I3) and a DFD motif that are distinct from other kinases (Figure 1). Crystal structures^{35,36} of the kinase domain of Mnk displays the typical bilobal arrangement of the catalytic domain of protein kinases, with the ATP binding cleft sandwiched between a N-terminal and a C-terminal lobe (Figure S1, Supporting Information). The N-terminal lobe contains a twisted sheet of five antiparallel β-strands (β1–β5) and the regulatory helix αC. It harbors the

elements essential for ATP binding such as the glycine-rich P-loop (residue 51–62 in Mnk1 and 86–97 in Mnk2), a conserved lysine (Lys78 in Mnk1 and Lys113 in Mnk2) in strand β3 and a conserved glutamic acid (Glu94 in Mnk1 and Glu129 in Mnk2) in helix αC; a salt bridge between these lysines and glutamic acids is a key feature of the active conformations of kinases. The predominantly α-helical C-terminal lobe contains the elements required for peptide substrate binding and phosphate transfer, including the catalytic loop (C-loop, residues 169–175 in Mnk1 and 204–210 in Mnk2), the magnesium-binding loop, and the activation segment (residues 191–225 in Mnk1 and 226–260 in Mnk2). Mnk1/2 possess a noncanonical DFD motif (Asp191–Phe192–Asp193 in Mnk1 and Asp226–Phe227–Asp228 in Mnk2) that lies within the magnesium-binding loop, replacing the DFG (Asp–Phe–Gly) motif typically found in other kinases. The DFD fingerprint is unique within the human kinome. Four different crystal structures are available for Mnk1/2. The structure of Mnk1 shows an autoinhibited form (PDB id 2HW6, resolution 2.6 Å)³⁶ (Figures 2 and S1), where Phe230 from the Mnk specific insertion region occupies a hydrophobic pocket; this pocket is normally occupied by Phe from the DFG motif in the active conformation of other kinases. The insertion of Phe230 into the hydrophobic pocket induces Phe192 of the DFD motif to flip out of the hydrophobic pocket, yielding the Mnk1 kinase in DFD-out (inactive) conformation; the Phe230 occludes the pocket from binding ATP. The wildtype structure of Mnk2 kinase has also been resolved in its DFD-out conformation and is incompatible with ATP binding (PDB id 2AC3, resolution 2.1 Å)³⁵ (Figures 2 and S1). However, unlike Mnk1, the structure of Mnk2 does not show an autoinhibited state and has an unusually extended activation loop conformation. In addition, the crystal structures of the Asp228Gly mutant form of Mnk2 are available both in apo (PDB id 2AC5, resolution 3.5 Å)³⁵ (Figure 2C) and staurosporine-bound forms (PDB id 2HW7, resolution 2.71

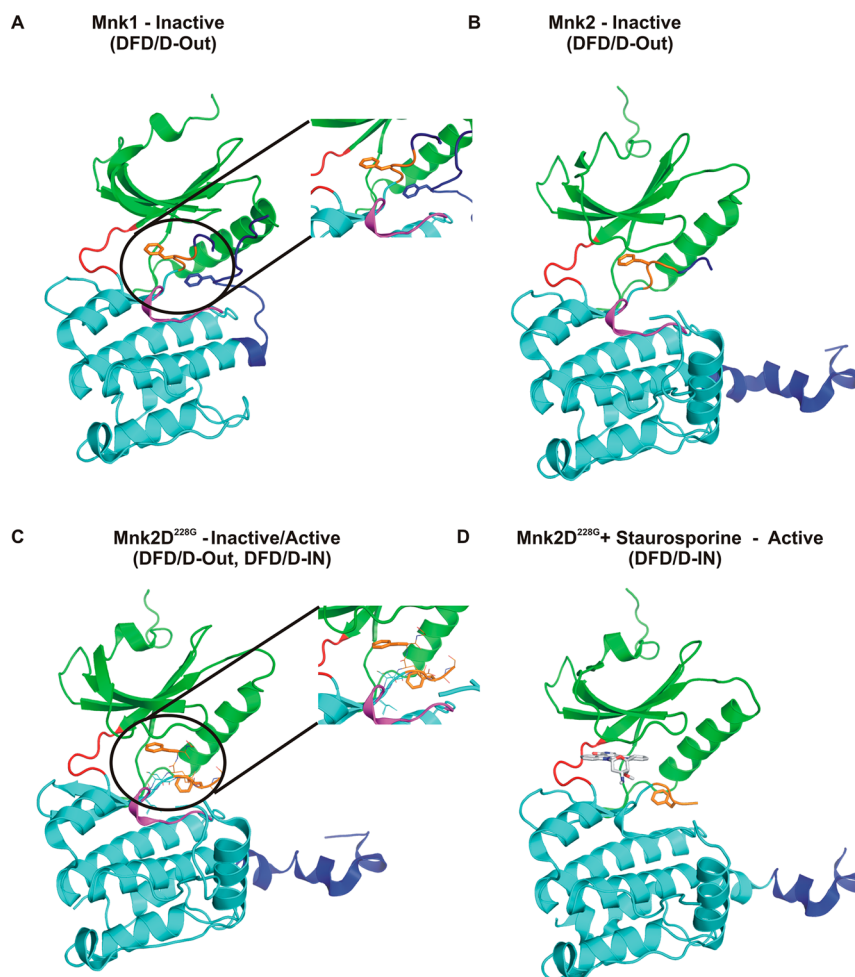


Figure 2. Crystal structures of Mnk1 and Mnk2 kinases. Cartoon representations of the overall structures of the kinase domains with prominent structural elements colored differently: N-terminal lobe (green), C-terminal lobe (cyan), hinge region (red), catalytic loop (magenta), DFD motif (orange), activation segment (blue). (A) Structure of Mnk1 (PDB id 2HW6) in its autoinhibited form. The Phe230 from the Mnk specific insertion and Phe192 from the DFD motif are shown as sticks. (B) Structure of Mnk2 (PDB id 2AC3) in its inactive (DFD-out) conformation; the Phe227 from the DFD motif is shown as sticks. (C) Structure of Mnk2^{D228G} (PDB id 2AC5) in its apo form, with the DFG motif (Phe227 shown as sticks) adopting both the active and inactive conformations. (D) Structure of Mnk2^{D228G} (PDB id 2HW7) bound with staurosporine (shown as gray sticks) with the DFG motif in the active conformation.

Å)³⁶ (Figure 2D); staurosporine is a promiscuous kinase inhibitor that binds to the active conformations of kinases. The Mnk2 mutant, with the second Asp in the unusual Mnk specific DFD motif mutated to glycine (DFG) crystallizes in both the DFG-in and the DFG-out conformations. Interestingly in both the Mnk kinases the DFD motif adopts a DFD-out (inactive) conformation, and such an inactive conformation, especially in the absence of ligands, is rarely observed in kinases.

Since the DFD-out conformation of Mnk1/2 prevents ATP binding, it may also prevent binding of ATP-competitive inhibitors. The majority of small-molecule kinase inhibitors developed so far act as ATP competitors targeting the ATP binding site, with their respective kinases adopting an active conformation. These inhibitors are referred as type I kinase inhibitors.³⁷ A second class of inhibitors that bind and stabilize the inactive DFG-out conformation are called type II kinase inhibitors.³⁸ Several ATP competitive inhibitors targeting a variety of kinases have been successfully developed as therapeutics.^{37–39} Recently a series of ATP competitive Mnk kinase inhibitors, all with inhibitory activity in the range of 18 nM to >10000 μ M have been developed in house.⁴⁰ In the current work, we use various computational methods to

investigate the binding of these inhibitors to the catalytic domains of Mnk kinases. Computational docking combined with molecular dynamics (MD) simulations is routinely used in current structure-based drug design strategies. The available crystal structures of wildtype Mnk kinases exist in an inactive (DFD-out) form that is not compatible for the binding of ATP and most ATP-competitive inhibitors (Figure 2). Although a crystal structure of the Asp228Gly mutant Mnk2 structure exists in an active (DFG-in) conformation (Figure S1, Supporting Information), it lacks density for most of the activation loop (A-loop) and Mnk specific insertions. Hence, we constructed homology models of the complete catalytic domains of Mnk1/2 and refined them with all atom MD simulations. The ATP competitive inhibitors developed in house were docked to the refined ensembles of the Mnk1/2 structures. The stability, dynamics, and binding energetics of these modeled Mnk–inhibitor complexes were further investigated using MD simulations.

MATERIALS AND METHODS

Homology Modeling. There are currently no crystal structures available for wildtype Mnk1/2 kinases in their active conformations. Hence, structures were constructed using comparative modeling methods based on homology. Sequence analysis shows that Mnk1 and Mnk2 kinases share ~33% and 38% sequence identity (~48% and 52% sequence similarity) respectively with the death associated protein kinase 1 (DAPK1); the three Mnk specific insertions (I1, I2, and I3) are unique to the Mnk kinases. DAPK1 being the protein with the highest sequence identity to the Mnk kinases and having been crystallized in an active form, we use it as a template for homology modeling. A high resolution (1.4 Å) crystal structure of the kinase domain of the active conformation of DAPK1 in its apo form (PDB code 1JKS)⁴¹ was used as the template to construct the three-dimensional models of the kinase domains of the two Mnk kinases. Although the sequence identity between the Mnk kinases and DAPK1 is relatively modest, it is well-known that the structural folds of the kinases are conserved.⁴² In addition, the models were also guided by the available crystal structures of Mnk kinases which have been resolved only in their inactive conformations were also used as templates. The program Modeler (version 9.12)⁴³ was used for generation of the homology models. Several models were generated and the models with the best physicochemical properties were refined further using all atom MD simulations.

MD Simulations. MD simulations were carried out to refine the homology models of the Mnk kinases and the predicted Mnk-inhibitor complexes (see next sections). MD simulations were carried out with the *Sander* module of the program Amber11.⁴⁴ The partial charges and force field parameters for each inhibitor were generated using the *Antechamber* module in Amber. All atom versions of the Amber 03 force field (ff03)⁴⁵ and the general Amber force field (GAFF)⁴⁶ were used for the protein and the inhibitors, respectively. The *Xleap* module was used to prepare the system for the MD simulations. All the simulation systems were neutralized with appropriate numbers of counterions. Each neutralized system was solvated in an octahedral box with TIP3P⁴⁷ water molecules, leaving at least 10 Å between the solute atoms and the borders of the box. All MD simulations were carried out in explicit solvent at 300 K. During the simulations, the long-range electrostatic interactions were treated with the particle mesh Ewald⁴⁸ method using a real space cutoff distance of 9 Å. The *Settle*⁴⁹ algorithm was used to constrain bond vibrations involving hydrogen atoms, which allowed a time step of 2 fs during the simulations.

Solvent molecules and counterions were initially relaxed using energy minimization with restraints on the protein and inhibitor atoms. This was followed by unrestrained energy minimization to remove any steric clashes. Subsequently the system was gradually heated from 0 to 300 K using MD simulations with positional restraints (force constant: 50 kcal mol⁻¹ Å⁻²) on protein and inhibitors over a period of 0.25 ns allowing water molecules and ions to move freely. During an additional 0.25 ns, the positional restraints were gradually reduced followed by a 2 ns unrestrained MD simulation to equilibrate all the atoms. For the refinement simulations, three independent MD simulations (assigning different initial velocities) were carried out on each equilibrated Mnk1/2 structure for 100 ns with conformations saved every 10 ps. For each Mnk1/2-inhibitor complex, a 10 ns production MD run

was carried out from the equilibrated structures, with conformations saved every 4 ps. A total of 50 Mnk1/2-inhibitor complexes were each subjected to this protocol.

Cluster analysis of the sampled conformations was performed using the *kclust* program in MMTSB-tools.⁵⁰ Simulation trajectories were visualized using VMD,⁵¹ and figures were generated using Pymol.⁵²

Ligand Preparation. The inhibitory activities of 25 imidazopyridine and imidazopyrazine derivatives that are developed in house are summarized in Table 1. The 3D structures of the inhibitors were built using *Maestro* and minimized using the *Macromodel* module employing the OPLS-2005 force field⁵³ in Schrödinger 9.0.⁵⁴ All the inhibitors were then prepared with *Ligprep* that generates low energy tautomers and enumerates realistic protonation states at physiological pH.

Ligand Docking. The prepared inhibitors were docked into the binding pockets of the models of Mnk1/2 kinases using *Glide*.⁵⁵ A box of size 10 × 10 × 10 Å for molecular docking, corresponding to the “inner-box” in *Glide*, centered on the selected active site residues was used to confine the search space of each docked ligand. For the grid generation, the default *Glide* settings were used. A rigid receptor docking (RRD) protocol was used which fixes the protein conformation while allowing the ligands to be flexible. All 25 inhibitors were docked into the active sites of Mnk1/2 kinases using this protocol, and the docked conformation of each ligand was evaluated using the *Glide* Extra Precision (XP) scoring function. Docking was carried out on several conformational substates of the Mnk kinases identified by clustering of MD trajectories. Because of the high flexibility of the loops, several clusters were generated; however only the top six were populated with 10–23% of the sampled conformations. Therefore, for the docking, for each kinase, six conformations representing the centroid of the six most highly populated clusters respectively were used. Two types of docking were examined: (a) unconstrained; (b) constrained, where a hydrogen bond between the backbone amide nitrogen of Leu127 in Mnk1 and Met162 in Mnk2 with any acceptor in the ligand atoms was imposed.

MMPBSA Calculations. The Molecular Mechanics Poisson–Boltzmann Surface Area (MMPBSA) methodology has been widely used to investigate the docking of ligands to receptors.^{56–58} We applied it to calculate the binding free energies between the Mnk1/2 and inhibitors. A total of 250 conformations were extracted from the last 5 ns of the MD simulations of each Mnk1/2-inhibitor complex. The MMPBSA calculations were carried out after removing the water molecules and the counterions. Binding free energies were calculated using the single trajectory method, based on the assumption that the bound and unbound conformations of the protein and inhibitor are quite similar. In this protocol, the isolated conformations of the inhibitor and the protein were extracted from the corresponding protein–inhibitor complex. For each conformation, the binding free energy (ΔG_{bind}) of the inhibitor to the protein was calculated as follows:

$$\Delta G_{\text{bind}} = G_{\text{complex}} - (G_{\text{receptor}} + G_{\text{ligand}}) \quad (1)$$

The binding free energy is estimated as a sum of three terms:

$$\Delta G_{\text{bind}} = \Delta G_{\text{MM}} + \Delta G_{\text{sol}} - T\Delta S \quad (2)$$

where ΔG_{MM} is the change in the molecular mechanics energy upon complexation in the gas phase, ΔG_{sol} is the change in solvation free energy, and $T\Delta S$ is the change of conformational entropy associated with ligand binding.

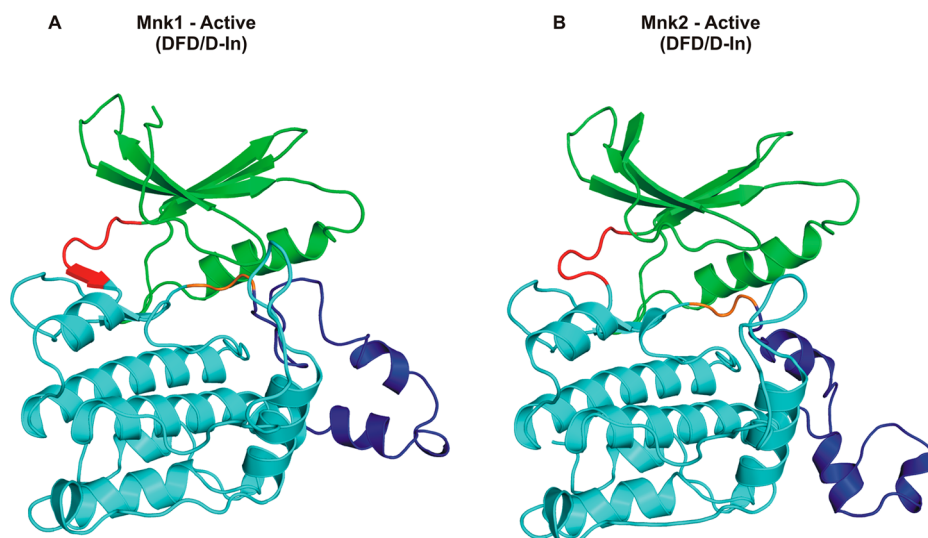


Figure 3. Homology models of (A) Mnk1 and (B) Mnk2 kinases. Cartoon representations of the overall structures of the kinase domains with prominent structural elements highlighted: N-terminal lobe (green), C-terminal lobe (cyan), hinge region (red), catalytic loop (magenta), DFD motif (orange), activation segment (blue). The activation loop in both the kinases is modeled in an extended conformation.

The molecular mechanics free energy (ΔG_{MM}) is further split into van der Waals (ΔG_{vdw}) and electrostatic (ΔG_{ele}) energies:

$$\Delta G_{MM} = \Delta G_{ele} + \Delta G_{vdw} \quad (3)$$

The solvation free energy ΔG_{sol} arises from polar (electrostatic) solvation free energy (ΔG_{PB}) and nonpolar solvation free energy (ΔG_{SA}) as in eq 4:

$$\Delta G_{sol} = \Delta G_{PB} + \Delta G_{SA} \quad (4)$$

ΔG_{PB} is computed by solving the linearized Poisson–Boltzmann (PB) equation using Parse radii and a solvent probe radius of 1.4 Å. In our calculations, the dielectric constant was set to 1.0 for the interior of the solutes and 80.0 for the solvent. ΔG_{SA} was determined using a solvent accessible surface area (SASA)–dependent term as in eq 5:

$$\Delta G_{SA} = \gamma \times \text{SASA} + \beta \quad (5)$$

where γ is the surface tension proportionality constant and was set to 0.00542 kcal/(mol·Å²), and β is the offset value, which was 0.92 kcal/mol here.

The entropy term ($-T\Delta S$) was computed under the harmonic approximation using the *Nmode* module in Amber 11.

Per-Residue Decomposition. In order to detect the “hot spot” residues, the effective binding energies were decomposed into contributions of individual residues using the MMGBSA energy decomposition scheme. The MMGBSA calculations were carried out in the same way as in the MMPBSA calculations. The polar contribution to the solvation free energy was determined by applying the generalized born (GB) method (igb = 2),⁴⁴ using mbondi2 radii. The nonpolar contributions were estimated using the ICOSA method⁴⁴ by a solvent accessible surface area (SASA) dependent term using a surface tension proportionality constant of 0.0072 kcal/mol Å².

To investigate the impact of mutational effects on ligand binding, selected residues were computationally mutated to alanine. The free energy changes ($\Delta\Delta G_{bind}$) were defined as $\Delta G_{bind}(\text{mutant}) - \Delta G_{bind}(\text{Wt})$ for a potential mutation from wildtype to mutant. A positive $\Delta\Delta G_{bind}$ indicates that ligand binding to the wildtype protein is more favorable, while

negative $\Delta\Delta G_{bind}$ indicates that ligand binding to the (alanine) mutant protein is more favorable.

RESULTS AND DISCUSSION

Homology Modeling, Refinement and Ensemble Generation. The available crystal structures of wildtype Mnk1 and Mnk2 are in their inactive conformations and are structurally incompatible for binding ATP or ATP-competitive inhibitors. Hence the structures of wildtype Mnk1/2 in their active conformations (DFD-in) were constructed by homology modeling using (~30% amino acid identity) the 3D structure of the death-associated protein kinase 1 (DAPK1; PDB id 1JKS, resolution 1.4 Å)⁴¹ which is another member of the CaMK group. The structure of DAPK1 also shows an unusually extended activation loop conformation, similar to the one that Mnk2 adopts in its inactive state (PDB id 2AC3, Figure 2B). In addition to the structure of DAPK1, the crystal structures of wildtype and mutant Mnk were also used as templates during the homology modeling process. Several models were generated using single and multiple templates, and the model with the best physicochemical properties was chosen for further use. The activation loop was assumed to be in the extended conformation and was thus modeled. The selected models show good structural similarity to the templates, with an average rmsd of ~1.3–1.5 Å. The generated models of Mnk1/2 (Figure 3) were further refined using all atom MD simulations in explicit solvent. For each kinase model, three independent MD simulations were performed assigning different initial velocities, and each simulation was carried out for 100 ns. During the MD simulations, the sampled conformations deviate from their initial conformations to about ~5–6 Å by ~20–25 ns (Figure S2, Supporting Information) after which they are relatively stable. This is due to large conformational changes that the activation loops undergo, but the other parts of the kinases stay relatively close to their starting conformations with an rmsd of ~2–3 Å throughout the simulations (Figure 4).

The conformations sampled during the last 50 ns of the MD simulations were clustered into conformational substates using the Kclust program from the MMTSB tool set,⁵⁰ with an rmsd of 2 Å set as cutoff. The cluster centroids of the top five most

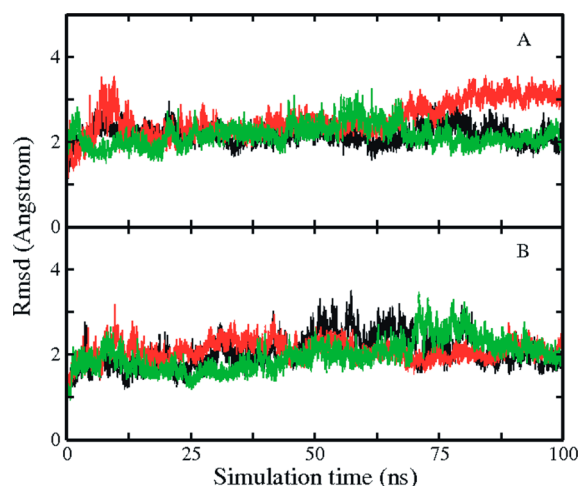


Figure 4. Refinement of the homology models of Mnk1 and Mnk2. Root mean square deviation (rmsd) of conformations sampled during three independent (black, red, green) MD simulations of 100 ns starting from the constructed homology models of Mnk1 (A) and Mnk2 (B). Rmsd is calculated for all residues except the activation loop/segment (residues 169–175 in Mnk1 and 226–260 in Mnk2) by superimposing all the residues with the respective homology models.

populated clusters of both Mnk kinases show that the secondary structural elements are quite similar, with large structural differences localized to the loop regions, particularly the activation loop. In addition the glycine rich P-loop also adopts two major conformations (open and close). The highly conserved glycine rich P-loop adopts an open conformation in most of the kinases in their ligand free/apo forms, and a closed conformation in the ligand/ATP-bound forms.^{59,60} Since the conformations of the activation loop and P-loop of Mnk kinases in their inhibitor bound states are not known, different conformations of the activation loop and P-loop identified by clustering were considered for the docking studies. The active state is retained during the simulations of the kinases in their apo as well as in their complexed states. This is not surprising

given that to witness conformational changes between the active and inactive states during simulations, either extremely long (by current capabilities) simulations⁶¹ or enhanced sampling methods⁶² are needed.

Binding Site Analysis. Both the Mnk1 and Mnk2 kinases share ~80% sequence identity within their catalytic domains and ~85% sequence identity in the canonical ATP binding pocket. Most of the residues in the catalytic sites of both the kinases are identical, with differences seen mainly in two regions (Figure 5): (a) the hinge region with residues Leu127 and Gln128 in Mnk1 replaced by Met162 and Arg163 respectively in Mnk2; (b) the glycine rich P-loop, where residues Thr51, Ser52, Glu53, Leu54, Tyr60, and Lys62 in Mnk1 are replaced by residues Gln86, Glu87, Asp88, Val89, His95, and Arg97 respectively in Mnk2. Nevertheless, the overall physicochemical properties of the canonical binding sites of Mnk1/2 kinases appear quite similar.

Ligand Docking. Recently a series of small molecule inhibitors that are derivatives of imidazopyridines (Table 1, left panel) and imidazopyrazines (Table 1, right panel) were designed and were shown to inhibit the activity of Mnk kinases.⁴⁰ The IC₅₀ values ranged from 18 nM to 10 μ M (Table 1). In order to model the binding of these small molecules to Mnk1/2, we docked them into the catalytic sites of Mnk1/2 kinases in their modeled active conformations (DFD-in). To account for receptor flexibility during the inhibitor docking process, representative structures were extracted after clustering the three 100 ns MD simulations of Mnk1/2 apo states. A docking protocol was developed and benchmarked by successfully redocking staurosporine into the crystal structure of the D228G mutant form of Mnk2. Initially, efforts at docking failed to correctly reproduce the experimentally observed binding mode of staurosporine as the top ranked or lowest energy conformation. However, imposing a constraint in the form of a hydrogen bond between staurosporine and the backbone amide of Met162 at the hinge region of the D228G mutant resulted in successful reproduction of the bound conformation (rmsd \approx 0.8 Å) between the docked and the

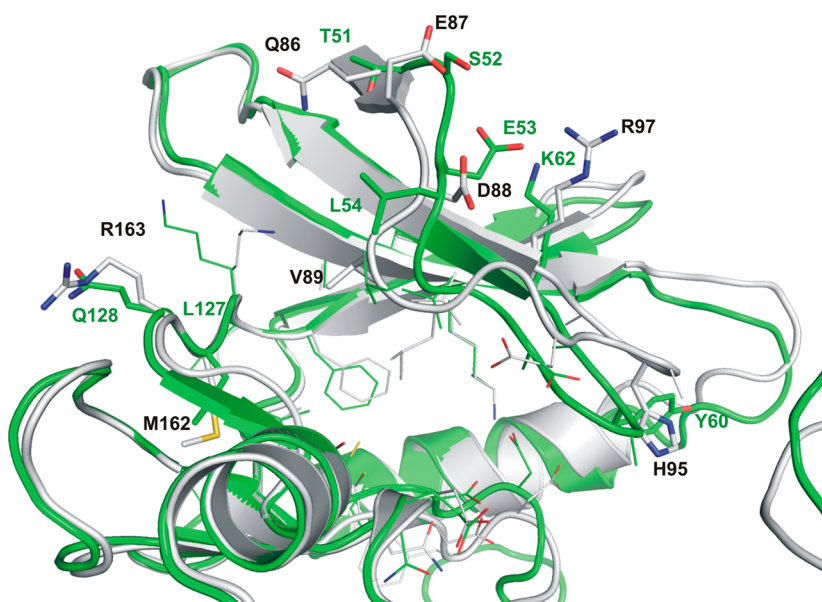
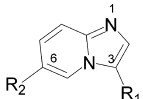
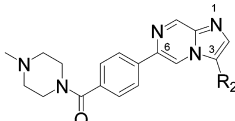
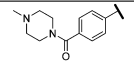
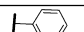
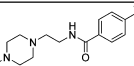
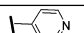
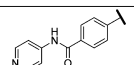
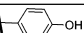
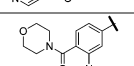

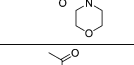
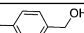
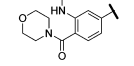
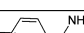
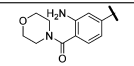
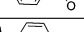
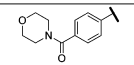
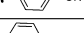
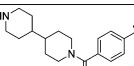
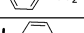
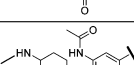
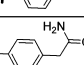
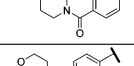
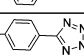
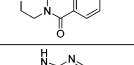
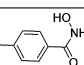
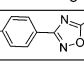


Figure 5. Binding sites of Mnk1 (green) and Mnk2 (gray). Active site residues that are similar in both the kinases are shown as lines. Residues that are different in both the kinases are highlighted as sticks and labeled accordingly.

Table 1. Structure and Activities of Imidazopyridine (Left Panel) and Imidazopyrazine (Right Panel) Derivatives^a

								
Compound #	R1	R2	Mnk1	Mnk2	Compound #	R2	Mnk1	Mnk2
1	4-PhOH		102	49	13		2684	1439
2	4-PhCN		206	123	14		2260	1831
3	4-PhCN		1416	231	15		55	39
4	4-PhCN		90	73	16		600	419
5	4-PhCN		99	77	17		1339	853
6	4-PhCN		330	384	18		294	187
7	4-PhCN		1787	1047	19		228	444
8	4-PhCN		23	18	20		4508	3131
9	4-PhCN		29	28	21		286	196
10	4-pyridyl		582	544	22		13920	9130
11	4-pyridyl		1914	1420	23		373	8294
12	4-PhCN		1137	1685	24		60	31
					25		>10000	>10000

^aActivities are given as inhibition constant (IC₅₀) values in nanomolar (nM).

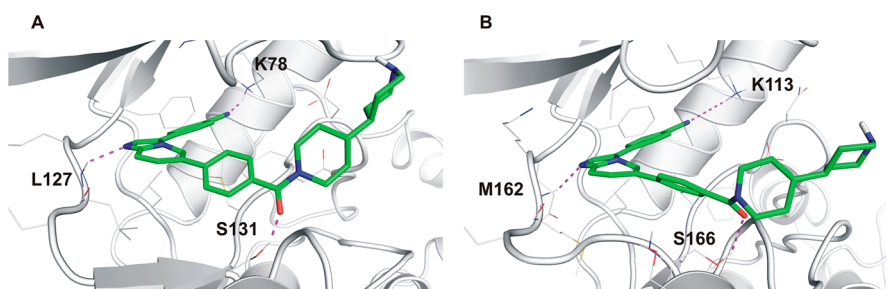


Figure 6. Predicted binding mode of compound 8, one of the imidazopyridine derivatives at the active sites of (A) Mnk1 and (B) Mnk2 kinase. Residues in the active sites of the kinases are shown as lines; hydrogen bonds are indicated by dashed lines (magenta); protein residues involved in hydrogen bond interactions are labeled accordingly.

experimental structures (Figure S3, Supporting Information) of staurosporine as the best docking pose in terms of energy. In addition, staurosporine also interacts with residues Glu160 and Glu209 through hydrogen bonds (Figure S3). We then evaluated the generated Mnk homology models for their ability to bind staurosporine. Although no bound structure of Mnk1 with staurosporine is available, owing to the similarity in the active sites between Mnk1/2, staurosporine was also expected to bind to Mnk1 in a manner similar to that in Mnk2. The docking protocol yielded docked poses of staurosporine in

wildtype Mnk1/2 kinase domains that were similar to the experimental conformation seen in the D228G form of Mnk2 (Figure S3).

Using this docking protocol, Mnk kinase inhibitors were docked into the catalytic sites of the active forms of the Mnk kinases. Although all dockings were carried out with and without hydrogen bond constraints, reasonable binding poses were observed only when the hydrogen bond constraints were imposed during docking. Docking calculations were repeated with different conformations of Mnk1/2 as identified through

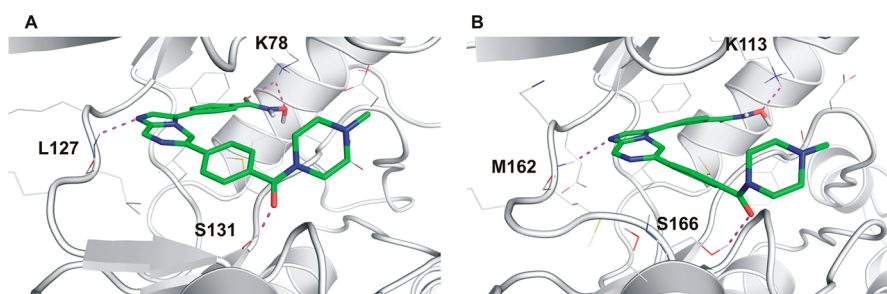


Figure 7. Predicted binding mode of compound **24**, one of the imidazopyrazine derivatives, at the active sites of (A) Mnk1 and (B) Mnk2 kinases. Residues in the active sites of the kinases are shown as lines; hydrogen bonds are indicated by dashed lines (magenta); protein residues involved in hydrogen bond interactions are labeled accordingly.

clustering the MD simulation trajectories. Ten poses for each compound were computed, and the best docking pose for each compound was chosen by ranking the computed binding energy (docking score). Analysis of the top scored solutions (lowest energy solutions) showed that all compounds bind similarly in the active sites of both kinases, with the core occupying the position occupied by adenine of ATP, and the two aromatic substituents occupying two pockets located next to the adenine-binding site. In addition, both derivatives are anchored to the hinge region of the kinases through hydrogen bonds and van der Waals contacts with residues from both the N- and C-terminal lobes of the kinases.

The imidazo[1,2-*a*]pyridine core or imidazo[1,2-*a*]pyrazine core occupies the adenine binding region in the active sites of both Mnk1 and Mnk2 (Figures 6 and 7). In both types of compounds the imidazole acceptor atom (N) hydrogen bonds with the amide backbone of the kinase hinge residue Leu127 in Mnk1 and Met162 in Mnk2.

The benzonitrile, phenol, or pyridine moieties (compounds **1**, **10**, and **11** respectively) of the imidazo[1,2-*a*]pyridine derivatives and a variety of functional groups substituted in the aromatic ring of the imidazopyrazine 3-position occupy the hydrophobic pocket formed by residues Phe124, Val63, Leu108, and Cys190 in Mnk1 and the homologous residues Phe159, Val98, Leu143, and Cys225 in Mnk2 (Figures 6 and 7). The nitrile nitrogen (compounds **2–9**, **12** and **19**) is within hydrogen bonding distance to the conserved catalytic Lys78 in Mnk1 and to Lys113 in Mnk2. Compound **1**, which has a phenol group, binds in the hydrophobic pocket, and the hydroxyl oxygen is within hydrogen bonding distance to the side chain of Lys78 in Mnk1 and of Lys113 in Mnk2. In the case of compounds **10** and **11** the pyridine group occupies the hydrophobic pocket. Some of the imidazopyrazine derivatives have substituents that are within hydrogen bonding distance to the conserved Lys78 in Mnk1 and Lys113 in Mnk2. Interestingly, only compounds that have substituents that can establish a hydrogen bond with the catalytic Lys78 in Mnk1 and Lys113 in Mnk2 show moderate to high binding affinities; in contrast, compounds lacking the ability to form this hydrogen bond are either weakly active or inactive (Table 1). In addition, the optimal size of the functional group that occupies the hydrophobic pocket is important, as compounds with large functional groups cannot be accommodated in this hydrophobic pocket due to steric clashes and thus have reduced potency.

The phenyl ring attached to the C-6 of the imidazopyridine and imidazopyrazine core is substituted with a wide variety of functional groups and notably a piperazine benzamide group. In all the compounds, the substituents at the 6-position occupy

the phosphate binding pocket close to the ATP ribose binding pocket. A major part of the inhibitor is buried inside the protein except the substituents at the 6-position, that interact with the glycine-rich P-loop and the loop connecting the hinge region and helix α D of the C-terminal lobe. For most of these compounds this phenyl group is substituted with a solubilizing group (either a morpholine or an alkylated piperazine) connected via an amide. The carbonyl oxygen of the amide is within hydrogen bonding distance of the side chain oxygen atom of Ser131 from Mnk1 and of Ser166 from Mnk2. This hydrogen bond seems important for the potency of these compounds, as compound **11**, lacking this hydrogen bond acceptor group, shows reduced activity, with IC_{50} values in the micromolar range.

We observed no correlation between the docking score and the experimentally determined IC_{50} values. The poor correlation between the docking scores and biological data is a major problem with current docking approaches.⁵⁶ Therefore, we employed a more sophisticated approach for the analysis of the key interactions necessary for high inhibitory activity.

MD Simulations. In order to investigate the stability of the modeled protein-inhibitor complexes and study their dynamics, MD simulations were carried out for 10 ns on each complex. The rmsd of protein atoms in the sampled protein-inhibitor complexes reached values of ~ 7 – 8 Å (Figure S4A,B) during the early stages of the simulations, arising mostly from the motions of the activation loop of the Mnk kinases. If the activation loop is excluded, the rmsd of the protein is stable with rmsd of ~ 2 – 2.5 Å (Figures 8A and S4C,D). A similar feature was observed in our simulations of the kinases in their apo states (see above). The increased flexibility of the activation loop is also seen in the root-mean-square fluctuation (rmsf) calculations (rmsf of the residues in the activation loop is ~ 9 Å and the rest of the protein is relatively stable with rmsf at ~ 3 Å). The compounds are also relatively stable with rmsd ~ 3 Å (Figures 8B and S5). No inhibitor unbinding was seen in any of the simulations, although recent studies suggest that this may occur at larger time scales.⁶³

The bound conformations of the inhibitors and the associated protein-inhibitor interactions as monitored through the distances between interacting atoms of the ligands and the protein binding sites (Figures S6 and S7) observed in the starting structures were generally maintained during the MD simulations. The hydrogen bonds in the ATP-binding pocket play a key role in kinase function and drug inhibition. The stability of the hydrogen bonding network predicted by *Glide* was examined as a function of the simulation time. The analysis of the MD trajectories of representative inhibitors indicates the presence of several hydrogen bonds between the inhibitors and

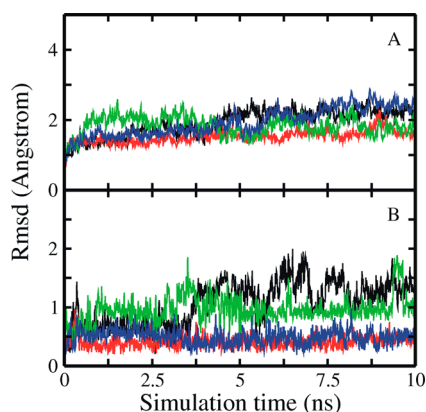


Figure 8. Rmsd of the sampled conformations of the Mnk–inhibitor complexes during the 10 ns MD simulations starting from the docked models. (A) rmsd of protein and (B) rmsd of compound **8** (black) and compound **24** (red) bound to Mnk1 and of compound **8** (green) and compound **24** (blue) bound to Mnk2. The protein rmsd is calculated excluding the activation loop/segment residues (residues 169–175 in Mnk1 and 226–260 in Mnk2).

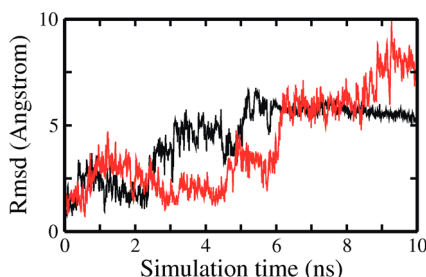


Figure 9. Rmsd of the sampled conformations of the inhibitor in the protein–inhibitor complexes during the 10 ns MD simulations starting from the docked models: rmsd of compound **11** in complex with Mnk1 (black) and Mnk2 (red).

the kinases with moderate to high frequencies. The hydrogen bond between the imidazole acceptor atom of the imidazopyridine or imidazopyrazine core and the backbone amide nitrogen of residues Leu127 in Mnk1 and Met162 in Mnk2 from the hinge region was well preserved throughout the simulation with 95% occupancy for all the simulated systems.

The benzonitrile group in compounds **2–9**, **12**, **19** and the different substituents at the 3-position on the aromatic ring of imidazopyrazine derivatives that occupy the hydrophobic pocket in Mnk1 and Mnk2 stay deeply buried in the hydrophobic pocket during the simulations. Interestingly, the

nitrogen atom of the benzonitrile group and the side chain amine of the catalytic lysine (Lys78 in Mnk1 and Lys113 in Mnk2) move closer to each other, yielding a stable hydrogen bond ($\sim 90\%$ occupancy). Compound **1**, which has a phenol instead of the benzonitrile group, occupies the hydrophobic pocket and interacts with this catalytic lysine through hydrogen bond for most part of the simulation ($\sim 80\%$ occupancy). Some of these substituents form stable hydrogen bonds with these conserved lysines in Mnk1/2. This hydrogen bond interaction seems to be important for potency as well as for stability of the protein–inhibitor complexes, as compounds **10**, **11**, and **14**, which all lack potential hydrogen bonding acceptors at this position display moderate to weak inhibitory activity, with IC_{50} mainly in the micromolar range. Moreover, the absence of this hydrogen bonding interaction renders some instability in the bound conformation of compounds **11** and **14**. Increased flexibility was observed for these compounds during the simulations, with the rmsd of compound **11** reaching values as high as ~ 8 Å compared to ~ 3 Å (Figure S4, Supporting Information) for the other ligands.

Different substitutions on the phenyl ring attached to the 6-position of imidazopyridine and imidazopyrazine core that occupy the phosphate pocket close to the ATP ribose binding site stay relatively stable during the simulations. The oxygen of the amides in para positions establishes a stable hydrogen bond ($\sim 80\%$ occupancy) interaction with the hydroxy group of Ser131 from Mnk1 and Ser166 from Mnk2 respectively during the simulations. In addition to the hydrogen bond made with the catalytic lysines seen above, this hydrogen bond also seems important for the potency and increased structural stability of the bound conformations of the imidazopyridine and imidazopyrazine derivatives.

Compounds **11** and **12** both lack this benzamide group and hence the hydrogen bond to Ser131/Ser166 from Mnk1/2 respectively and have reduced activity, with IC_{50} values in the micromolar range; they show increased flexibility in the simulations. Compounds **4**, **5**, **6**, and **9** carry substituents at the ortho or meta positions on the aromatic rings which occupies the ribose pocket. Compounds **5** and **9** have an additional amide substituent in the meta position which leads to the formation of a hydrogen bond between the oxygen atom of the amide and the side chain oxygen of Ser169 from Mnk2 (Figure 10); such a hydrogen bond interaction is not possible with Mnk1, as the Mnk1 kinase has Ala134 instead of Ser169 at this position. However, the oxygen atom of the amide from these compounds interacts with the backbone oxygen of Ser131 in Mnk1 through a water molecule. In general, increased flexibility was seen for all the compounds that have larger

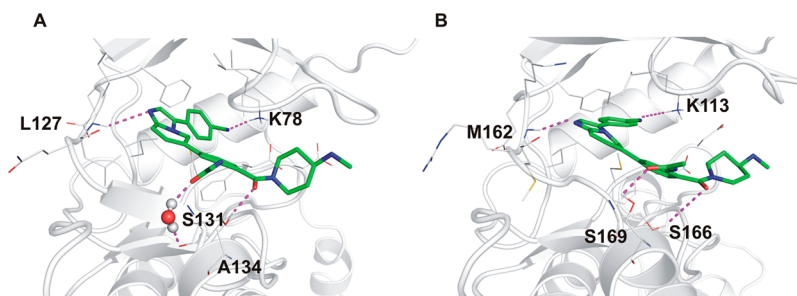


Figure 10. Structural snapshots showing the differences in interactions between an inhibitor (compound **9**) with the two kinases; residues in the active sites of the kinases are shown as lines; hydrogen bonding interactions between compound **9** and (A) Mnk1 and (B) Mnk2 kinases indicated by the dashed lines (magenta). The protein residues involved in hydrogen bond interactions are labeled accordingly.

Table 2. Binding Free Energies of Each MNK1–Inhibitor Complex Calculated by MMPBSA^a

compd	ΔE_{elec}	ΔE_{vdw}	ΔG_{SA}^b	ΔG_{PB}	$\Delta H_{(\text{PB})}^c$	$T\Delta S^d$	$\Delta G_{\text{pred(PB)}}^e$	pIC_{50}^f
1	−14.77	−49.35	−5.88	37.46	−32.54	−10.26	−22.28	6.99
2	−18.01	−49.99	−6.2	37.5	−36.69	−15.00	−21.69	6.69
4	−26.66	−59.09	−6.75	51.59	−40.92	−13.73	−27.19	7.04
5	−12.71	−56.02	−6.49	34.69	−40.53	−11.5	−29.03	7.00
6	−14.77	−53.54	−6.37	40.33	−34.35	−17.09	−17.26	6.48
7	−14.29	−49.79	−5.89	38.06	−31.91	−19.26	−12.65	5.75
8	−18.87	−54.27	−6.27	42.86	−36.55	−14.99	−21.56	7.64
9	−25.94	−56.32	−6.28	47.5	−41.04	−7.23	−33.81	7.54
10	−11.35	−47.01	−5.59	36.23	−27.72	−16.23	−11.49	6.24
12	−23.88	−48.16	−5.41	41.94	−35.51	−20.02	−15.49	5.94
13	−10.09	−47.83	−5.67	32.43	−31.16	−15.07	−16.09	5.57
15	−26.9	−49.06	−5.78	46.77	−34.98	−20.89	−14.09	7.26
16	−15.03	−53.69	−5.69	40.71	−33.7	−20.69	−13.01	6.22
17	−27.95	−45.55	−5.99	46.7	−32.8	−14.39	−18.41	5.87
18	−27.55	−49.38	−6.31	51.77	−31.46	−15.75	−15.71	6.53
19	−16.51	−52.36	−6.07	39.77	−35.17	−11.62	−23.55	6.59
20	−19.78	−42.00	−5.4	38.21	−28.97	−18.27	−10.7	5.34
21	−8.72	−47.33	−6.13	32.44	−29.73	−13.91	−15.82	6.54
22	−21.55	−49.76	−6.52	48.11	−29.73	−19.13	−10.6	4.86
23	−37.4	−51.39	−6.31	52.1	−43.01	−23.00	−20.01	6.47
24	−35.9	−52.75	−6.49	58.13	−36.97	−17.4	−19.57	7.22
25	−14.05	−47.42	−6.29	40.37	−27.39	−16.1	−11.29	<5.00

^aMean energies are in kcal/mol. ^b $\Delta G_{\text{SA}} = \gamma \times \text{SASA} + \beta$; $\gamma = 0.00542$ kcal/mol Å^{−2}; $\beta = 0.92$ kcal/mol. ^c $\Delta H_{(\text{PB})} = \Delta E_{\text{elec}} + \Delta E_{\text{vdw}} + \Delta G_{\text{SA}} + \Delta G_{\text{PB}}$. ^d $T\Delta S$ = entropy changes. ^e $\Delta G_{\text{pred(PB)}}$ (calculated binding free energy by MMPBSA method) = $\Delta H_{(\text{PB})} - T\Delta S$. ^f $\text{pIC}_{50} = (-\log \text{IC}_{50})$.

Table 3. Binding Free Energies of Each MNK2–Inhibitor Complex Calculated by MMPBSA^a

compd	ΔE_{elec}	ΔE_{vdw}	ΔG_{SA}^b	ΔG_{PB}	$\Delta H_{(\text{PB})}^c$	$T\Delta S^d$	$\Delta G_{\text{pred(PB)}}^e$	pIC_{50}^f
1	−20.83	−45.45	−5.96	42.43	−29.82	−3.098	−26.722	7.31
2	−8.39	−53.89	−6.42	30.66	−38.04	−19.25	−18.79	6.91
4	−0.88	−67.28	−6.66	31.71	−43.11	−21.14	−21.97	7.14
5	−18.62	−55.79	−6.73	43.91	−27.24	−10.42	−26.82	7.11
6	−9.79	−52.38	−6.2	32.81	−35.59	−12.35	−23.24	6.42
7	−9.6	−47.06	−5.92	28.4	−34.18	−17.98	−16.2	5.98
8	−13.48	−52.92	−6.08	33.59	−38.89	−11.49	−27.4	7.74
9	−15.47	−55.47	−6.55	39.69	−37.8	−10.91	−26.89	7.55
10	−12.6	−47.22	−5.64	34.43	−31.04	−7.58	−23.46	6.26
12	−9.67	−46.33	−5.46	29.88	−31.58	−13.99	−17.59	5.77
13	−8.5	−44.99	−5.46	29.32	−29.63	−22.8	−6.83	5.84
15	−20.14	−46.13	−5.63	37.46	−34.45	−10.43	−24.02	7.41
16	−9.67	−42.77	−5.66	30.82	−27.82	−12.76	−15.06	6.38
17	−19.53	−48.47	−6.06	42.00	−32.07	−11.58	−20.49	6.07
18	−20.02	−50.85	−6.08	43.45	−33.51	−15.69	−17.82	6.73
19	−7.1	−49.1	−6.07	31.63	−30.63	−14.03	−16.6	6.64
20	−8.14	−50.86	−6.26	34.20	−31.05	−17.99	−13.06	5.50
21	−9.46	−46.12	−5.93	30.44	−31.08	−13.71	−17.37	6.70
22	−26.33	−50.74	−6.12	52.82	−30.37	−14.78	−15.59	5.04
23	−28.89	−55.22	−6.36	49.08	−41.39	−27.88	−13.51	6.09
24	−35.86	−50.57	−6.04	53.53	−38.94	−19.4	−19.54	7.51
25	−20.69	−55.53	−6.45	44.20	−38.47	−27.71	−10.76	<5.00

^aMean energies are in kcal/mol. ^b $\Delta G_{\text{SA}} = \gamma \times \text{SASA} + \beta$; $\gamma = 0.00542$ kcal/mol Å^{−2}; $\beta = 0.92$ kcal/mol. ^c $\Delta H_{(\text{PB})} = \Delta E_{\text{elec}} + \Delta E_{\text{vdw}} + \Delta G_{\text{SA}} + \Delta G_{\text{PB}}$. ^d $T\Delta S$ = entropy changes. ^e $\Delta G_{\text{pred(PB)}}$ (calculated binding free energy by MMPBSA method) = $\Delta H_{(\text{PB})} - T\Delta S$. ^f $\text{pIC}_{50} = (-\log \text{IC}_{50})$.

substituents on the aromatic ring that occupies the ribose pocket.

MMPBSA Binding Free Energy Calculation. The binding free energies for the 44 imidazopyridine or imidazopyrazine derivative inhibitor complexes with Mnk1 and Mnk2 were calculated from the MD simulations using the MM-PBSA method described in the Materials and Methods. Compounds

3, 11, and 14 for which increased flexibility was observed during the simulations were not considered for the binding energy calculations.

The calculated binding free energies, individual energy terms, and the entropy changes of the 44 Mnk1/2 - imidazopyridine or imidazopyrazine derivatives are listed in Tables 2 and 3. The predicted binding affinities are in good agreement with the

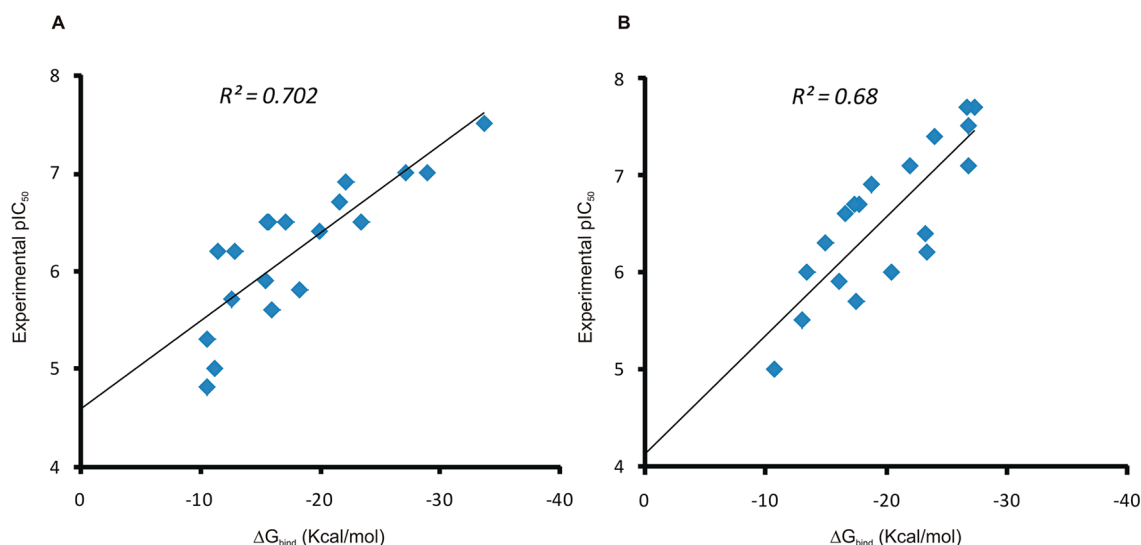


Figure 11. Correlation between the calculated MMPBSA binding free energies (ΔG_{bind}) and the experimental pIC_{50} values for (A) Mnk1 (B) Mnk2.

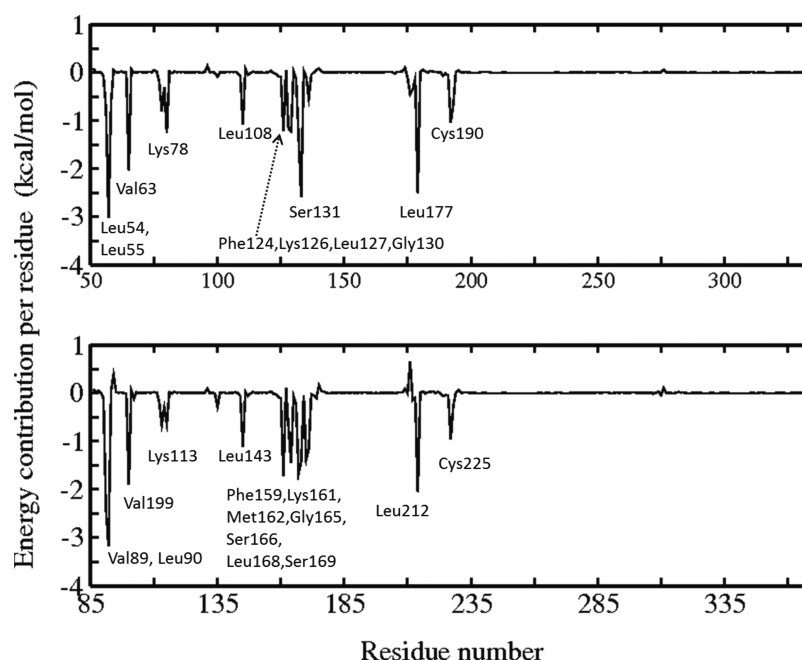


Figure 12. Decomposition of binding free energy on per residue basis for (top) Mnk1–compound 9 (the most potent of these series) (bottom) Mnk2–compound 9 complex.

experimental data. Binding free energies calculated with the MMPBSA approach do not reproduce the absolute experimental values, but they have been shown to correlate well with the experimental values.^{56–58} To further investigate the usefulness of the MMPBSA approach to discriminate between weak and strong Mnk inhibitors, the correlation between calculated binding free energies and the experimental pIC_{50} values of the ligands was analyzed. It is clear that this approach represents only a rough approximation, as biological data from an in vitro assay are used instead of pure thermodynamic values from calorimetric studies. Therefore, an ideal correlation is not expected. When only the enthalpic part of the free energy is considered (ΔH), a correlation ($r^2 = 0.44$ and 0.34 for Mnk1 and Mnk2 respectively) was observed between the predicted enthalpy of binding and the biological activity data. When the entropy term ($T\Delta S$) calculated using the harmonic approx-

imation in normal mode analysis (NMA) is included, a significant improvement in the correlation was observed ($r^2 = 0.51$ and 0.56 for Mnk1 and Mnk2); removal of two outliers further improved this (Figure 11A,B) approximately linear relationship (correlation coefficient, $r^2 = 0.70$ and 0.68 ; Figure 11A,B).

In all 44 complexes, van der Waals, electrostatics, and nonpolar solvation terms are quite favorable for inhibitor binding to Mnk1/2 kinases, while the polar solvation and entropy terms are unfavorable for binding. We then compared the correlation between the predicted binding free energies and each energy component. We found that the nonpolar contributions (Vdw + SA) correlated better with the experimental activity data, suggesting that the nonpolar contributions, especially the van der Waals energies, contribute the most to the binding free energy for each complex (~ -65

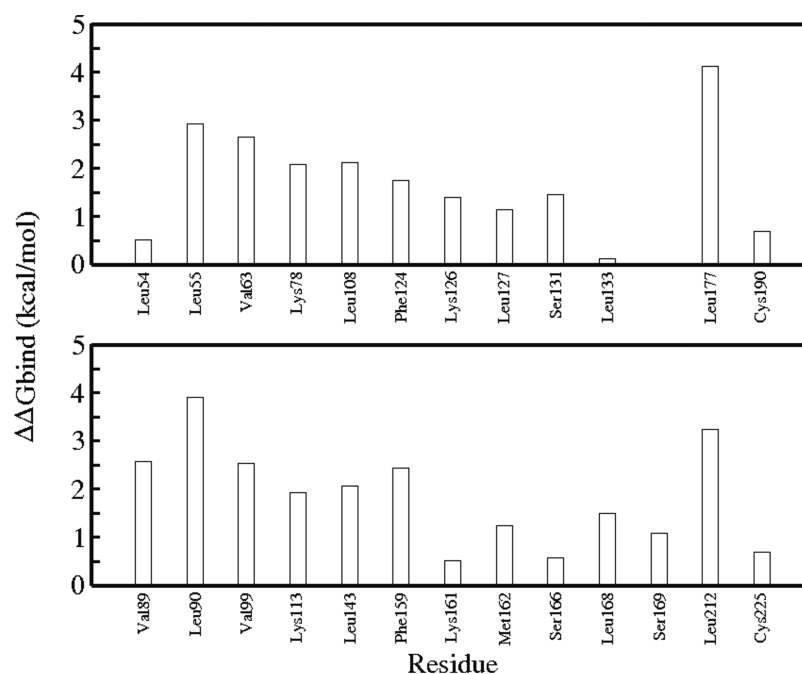


Figure 13. Results of alanine scanning. Mutational effects of selected amino acid residues of the Mnk1 (top) Mnk2 (bottom) binding pocket on the calculated free energies for the binding of the most potent Compound 9 to Mnk1/2.

to -42 kcal/mol). This indicates that van der Waals/hydrophobic interactions are most significant in stabilizing the kinase–inhibitor complexes and that shape complementarity is the primary factor that dominates the affinities of these inhibitors binding to Mnk kinases. The nonpolar interaction is a key component that determines the difference of the binding affinities, as this term is significantly more negative for the most active compounds (~ -62.6 kcal/mol) than for the inactive compounds (~ -52.3 kcal/mol). Of course it also must be pointed out that the nonpolar part together with the hydrogen bond short-range interactions are the part of the free energy that is most accurately computed. This arises from the limitations of the fixed charge models and hence the lack of polarization effects in the classical electrostatic models employed here.

The polar energy term (ΔG_{elec}) is unfavorable for binding in all the complexes studied here, suggesting that the desolvation penalties imposed upon embedding the molecules into the cavities do not favor binding. The entropy term ($-T\Delta S$) has a magnitude comparable to the electrostatic interactions. Hence, it also plays an important role in determining the binding free energy of the inhibitor binding to the Mnk kinases. Our results show loss of entropy for all Mnk–inhibitor complexes. It is not surprising since the ligands are more flexible in solution than upon being sequestered in the complexes.

Decomposition Analysis of the Binding Free Energy.

In order to gain further insights into the energetic contributions of individual residues to complex formation, the binding free energies (interaction energies) were decomposed on a per-residue level using the MMGBSA approach. The decomposition of the relative free energies revealed that all these complexes have similar interaction patterns (Figure 12), which further supports the observation of the inhibitors adopting very similar binding modes. The most favorable interactions are formed by residues in the active sites of the kinases. Residues Leu54, Leu55, Val63, Leu108, Phe124, Leu177 from Mnk1 and Val89, Leu90, Val99, Leu143, Phe159, Leu212 from Mnk2

contribute the most, indicating that the hydrophobic interactions are most critical for inhibitor binding. In addition, residues Lys78, Ser131 from Mnk1, Lys113, Ser166 from Mnk2 and hinge region residues Lys126, Leu127 and Lys161, Met162 from Mnk1 and Mnk2, respectively, interact with the inhibitor through H-bonds and contribute significantly to the interaction energies.

Computational alanine scanning was employed to determine the role of active site residues on ligand binding. The computational mutagenesis was done with the single-trajectory method. The trajectories of the wild-type Mnk1/2–inhibitor complexes were used to generate the structures of the mutated Mnk1/2–inhibitor complexes. This method depends on the assumption that the effects of mutating a residue to alanine only propagate locally and will result in insignificant entropic changes. For alanine scanning only those residues that contribute significantly (>1 kcal/mol) to the effective energy were considered. Nine key residues excluding glycine and alanine forming the walls of the binding pocket were mutated (Figure S8, Supporting Information), and the results of the mutagenesis are presented. Changes in the inhibitor–residue interactions associated with the alanine scan show that in general mutations of active site residues are highly unfavorable with all the inhibitors studied here (Figure 13). Unsurprisingly, significant losses in binding free energies were observed mainly for the hydrophobic residues, with van der Waals components the most affected. In addition, K78A (K113A in Mnk2) mutated complexes undergoes a substantial destabilization as the mutation removes a key H-bond between the side chain of Lys78 (Lys113 in Mnk2) and the inhibitor, responsible for stability and potency. Similarly the mutation of Ser131 in Mnk1 and Ser166 in Mnk2 also results in destabilization of the ligand bound complex. In the case of Mnk2, serine residue 169 contributes ~ 1.0 kcal mol $^{-1}$; in contrast this is replaced by Ala in Mnk1. Mutation of hinge residues Lys126, Leu127 in Mnk1 and Lys161, Met162 in Mnk2 to alanine has only a moderate

effect, since these residues interact with the inhibitor through H-bonds with their backbone atoms.

CONCLUSIONS

In this study an integrated computational approach that combines homology modeling, molecular docking, MD simulations, and MMPBSA binding free energy calculations was used to characterize the interactions between Mnk1/2 and a series of imidazopyridine and imidazopyrazine based inhibitors. Homology models of Mnk1/2 in their active conformations (DFD-in) were constructed and refined using all atom MD simulations in explicit solvent. A series of imidazopyridine and imidazopyrazine derivatives were docked into the active sites of Mnk1/2 kinases. Our docking calculations revealed that all compounds bind deeply inside the ATP binding sites with very similar binding modes. The imidazopyridine and imidazopyrazine cores occupy the adenine region and are anchored to the kinase hinge through hydrogen bonds. The substituents on both sides of the core groups occupy the hydrophobic pocket, ribose pocket, and phosphate binding pockets. MD simulations further revealed that the predicted protein–inhibitor complexes are very stable, with most of the interactions observed in the docking models well preserved. In addition, MD simulations show that hydrogen bonding interactions between the inhibitors and the catalytic Lys78, Ser131 (Mnk1), and Lys113, Ser166 (Mnk2) from the ribose pocket are important for the stability of the bound conformations of the ligands. In addition to maintaining hydrophobic interactions, these stable hydrogen bonds appear to be important for increased affinity of inhibitors by increasing the electrostatic interaction energies. The binding free energies predicted using MMPBSA calculations are largely consistent with the experimental data, yielding a reasonable ranking of binding affinities. Further decomposition of components of the binding free energy suggests that van der Waals and nonpolar solvation terms are the major contributors for the binding of these small molecule inhibitors to the Mnk1/2 kinases. In addition entropy changes also play an indispensable role in determining the binding free energies of these compounds. Residue-level decomposition of binding energies and computational alanine scanning reveals that mostly the hydrophobic residues at the active sites of the Mnk kinases are the major determinants of the binding of these small molecule inhibitors. In summary the findings in this work provide detailed structural understanding of a set of imidazopyridine and imidazopyrazine inhibitors targeting the DFD-in form (active form) of the Mnk1/2 kinases and offer a basis for further rational design of new potent inhibitors.

ASSOCIATED CONTENT

Supporting Information

Figure S1: Cartoon representation of crystal structures of Mnk1 and Mnk2 kinases. Figure S2: Rmsd of homology models of Mnk1 and Mnk2 conformations; Figure S3: Structural comparison between the docked conformations of staurosporine with its experimentally observed bound conformation. Figure S4: Rmsd of Mnk1/2 conformations sampled during Mnk1/2–inhibitor complex simulations. Figure S5: Rmsd of inhibitors conformations sampled during Mnk1/2–inhibitor complex simulations. Figures S6 and S7: Temporal evolution of Mnk1/2–inhibitors interactions. Figure S8: Binding pockets of Mnk1/2 highlighting residues that are mutated during the

alanine scanning. This material is available free of charge via the Internet at <http://pubs.acs.org>.

AUTHOR INFORMATION

Corresponding Authors

*(S.K.) E-mail: raghavk@bii.a-star.edu.sg. Tel: +65 6478 8353. Fax: +65 6478 9048.

*(C.S.V.) E-mail: chandra@bii.a-star.edu.sg. Tel: +65 6478 8273. Fax: +65 6478 9048.

Funding

This work was financially supported by Biomedical Sciences Institutes (BMSI) and Joint Council Office (JCO Project 11 03 FG 07 05), Agency for Science, Technology and Research (A*STAR), Singapore, which is gratefully acknowledged.

Notes

The authors declare no competing financial interest.

ACKNOWLEDGMENTS

The authors thank A*STAR Computing Resource Centre (A*CRC) for computing facilities.

REFERENCES

- (1) Watkins, S. J., and Norbury, C. J. (2002) Translation initiation and its deregulation during tumorigenesis. *Br. J. Cancer* 86, 1023–1027.
- (2) Lazaris-Karatzas, A., Montine, K. S., and Sonenberg, N. (1990) Malignant transformation by a eukaryotic initiation factor subunit that binds to mRNA 5' cap. *Nature* 345, 544–547.
- (3) Clemens, M. J. (2004) Targets and mechanisms for the regulation of translation in malignant transformation. *Oncogene* 23, 3180–3188.
- (4) Graff, J. R., and Zimmer, S. G. (2003) Translational control and metastatic progression: Enhanced activity of the mRNA cap-binding protein eIF-4E selectively enhances translation of metastasis-related mRNAs. *Clin. Exp. Metastasis* 20, 265–273.
- (5) De Benedetti, A., and Graff, J. R. (2004) eIF-4E expression and its role in malignancies and metastases. *Oncogene* 23, 3189–3199.
- (6) De Benedetti, A., and Harris, A. L. (1999) eIF4E expression in tumors: its possible role in progression of malignancies. *Int. J. Biochem. Cell Biol.* 31, 59–72.
- (7) Fan, S., Ramalingam, S. S., Kauh, J., Xu, Z., Khuri, F. R., and Sun, S. Y. (2009) Phosphorylated eukaryotic translation initiation factor 4 (eIF4E) is elevated in human cancer tissues. *Cancer Biol. Ther.* 8, 1463–1469.
- (8) Graff, J. R., et al. (2009) eIF4E activation is commonly elevated in advanced human prostate cancers and significantly related to reduced patient survival. *Cancer Res.* 69, 3866–3873.
- (9) Anthony, B., Carter, P., and De Benedetti, A. (1996) Overexpression of the proto-oncogene/translation factor 4E in breast-carcinoma cell lines. *Int. J. Cancer* 65, 858–863.
- (10) Ruggero, D., et al. (2004) The translation factor eIF-4E promotes tumor formation and cooperates with c-Myc in lymphomagenesis. *Nat. Med.* 10, 484–486.
- (11) Yoshizawa, A., et al. (2010) Overexpression of phospho-eIF4E is associated with survival through AKT pathway in non-small cell lung cancer. *Clin. Cancer Res.* 16, 240–248.
- (12) Nathan, C. A., Franklin, S., Abreo, F. W., et al. (1999) Expression of eIF4E during head and neck tumorigenesis: Possible role in angiogenesis. *Laryngoscope* 109, 1253–1258.
- (13) Topisirovic, I., Guzman, M. L., McConnell, M. J., et al. (2003) Aberrant eukaryotic translation initiation factor 4E-dependent mRNA transport impedes hematopoietic differentiation and contributes to leukemogenesis. *Mol. Cell Biol.* 23, 8992–9002.
- (14) Fraser, C., and Morley, S. (1997) Studies on the phosphorylation of eIF4E in *Xenopus* (XIK-2) kidney cells. *Biochem. Soc. Trans.* 25, 190S.

- (15) Rosenwald, I. B., Chen, J. J., Wang, S., Savas, L., London, I. M., and Pullman, J. (1999) Upregulation of protein synthesis initiation factor eIF-4E is an early event during colon carcinogenesis. *Oncogene* 18, 2507–2517.
- (16) Wang, S., Rosenwald, I. B., Hutzler, M. J., Pihan, G. A., Savas, L., Chen, J. J., and Woda, B. A. (1999) Expression of the eukaryotic translation initiation factors 4E and 2alpha in non-Hodgkin's lymphomas. *Am. J. Pathol.* 155, 247–255.
- (17) Nathan, C. O., Carter, P., Liu, L., Li, B. D., Abreo, F., Tudor, A., Zimmer, S. G., and De Benedetti, A. (1997) Elevated expression of eIF4E and FGF-2 isoforms during vascularization of breast carcinomas. *Oncogene* 15, 1087–1094.
- (18) McCubrey, J. A., Steelman, L. S., Kempf, C. R., et al. (2011) Therapeutic resistance resulting from mutations in Raf/MEK/ERK and PI3K/PTEN/Akt/mTOR signaling pathways. *J. Cell. Physiol.* 226, 2762–2781.
- (19) Waskiewicz, A. J., et al. (1999) Phosphorylation of the cap-binding protein eukaryotic translation initiation factor 4E by protein kinase Mnk1 in vivo. *Mol. Cell. Biol.* 19, 1871–1880.
- (20) Pyronnet, S. (2000) Phosphorylation of the cap-binding protein eIF4E by the MAPK-activated protein kinase Mnk1. *Biochem. Pharmacol.* 60, 1237–1243.
- (21) Knauf, U., Tschopp, C., and Gram, H. (2001) Negative regulation of protein translation by mitogen-activated protein kinase-interacting kinases 1 and 2. *Mol. Cell. Biol.* 21, 5500–5511.
- (22) Buxade, M., Parra-Palau, J. L., and Proud, C. G. (2008) The Mnk: MAP kinase-interacting kinases (MAP kinase signal-integrating kinases). *Front. Biosci.* 13, 5359–5373.
- (23) Flynn, A., and Proud, C. G. (1995) Serine 209, not serine 53, is the major site of phosphorylation in initiation factor eIF-4E in serum-treated Chinese hamster ovary cells. *J. Biol. Chem.* 270, 21684–21688.
- (24) Scheper, G. C., and Proud, C. G. (2002) Does phosphorylation of the cap-binding protein eIF4E play a role in translation initiation? *Eur. J. Biochem.* 269, 5350–5359.
- (25) Ueda, T., Sasaki, M., Elia, A. J., Chio, I. I., Hamada, K., Fukunaga, R., and Mak, T. W. (2010) Combined deficiency for MAP kinase-interacting kinase 1 and 2 (Mnk1 and Mnk2) delays tumor development. *Proc. Natl. Acad. Sci. U. S. A.* 107, 13984–13990.
- (26) Furic, L., et al. (2010) eIF4E phosphorylation promotes tumorigenesis and is associated with prostate cancer progression. *Proc. Natl. Acad. Sci. U. S. A.* 107, 14134–14139.
- (27) Hay, N. (2010) Mnk earmarks eIF4E for cancer therapy. *Proc. Natl. Acad. Sci. U. S. A.* 107, 13975–13976.
- (28) Lachance, P. E., Miron, M., Raught, B., Sonenberg, N., and Lasko, P. (2002) Phosphorylation of eukaryotic translation initiation factor 4E is critical for growth. *Mol. Cell. Biol.* 22, 1656–1663.
- (29) Wendel, H. G., et al. (2007) Dissecting eIF4E action in tumorigenesis. *Genes Dev.* 21, 3232–3237.
- (30) Wendel, H. G., et al. (2004) Survival signalling by Akt and eIF4E in oncogenesis and cancer therapy. *Nature* 428, 332–337.
- (31) Ueda, T., Watanabe-Fukunaga, R., Fukuyama, H., Nagata, S., and Fukunaga, R. (2004) Mnk2 and Mnk1 are essential for constitutive and inducible phosphorylation of eukaryotic initiation factor 4E but not for cell growth or development. *Mol. Cell. Biol.* 24, 6539–6549.
- (32) Hou, J., Kam, F., Proud, C., and Wang, S. (2012) Targeting Mnk for Cancer Therapy. *Oncotarget* 2, 118–131.
- (33) Lim, S., Saw, T. Y., Zhang, M., et al. (2013) Targeting of the MNK-eIF4E axis in blast crisis chronic myeloid leukemia inhibits leukemia stem cell function. *Proc. Natl. Acad. Sci. U. S. A.* 110, 2298–2307.
- (34) Waskiewicz, A. J., Flynn, A., Proud, C. G., and Cooper, J. A. (1997) Mitogen-activated protein kinases activate the serine/threonine kinases Mnk1 and Mnk2. *EMBO J.* 16, 1909–1920.
- (35) Jauch, R., Jakel, S., Netter, C., Schreiter, K., Aicher, B., Jackle, H., and Wahl, M. C. (2005) Crystal structures of the Mnk2 kinase domain reveal an inhibitory conformation and a zinc binding site. *Structure* 13, 1559–1568.
- (36) Jauch, R., Cho, M. K., Jakel, S., Netter, C., Schreiter, K., Aicher, B., Zweckstetter, M., Jackle, H., and Wahl, M. C. (2006) Mitogen-activated protein kinases interacting kinases are autoinhibited by a reprogrammed activation segment. *EMBO J.* 25, 4020–4032.
- (37) Zuccotto, F., Ardini, E., Casale, E., and Angiolini, M. (2010) Through the "gatekeeper door": exploiting the active kinase conformation. *J. Med. Chem.* 53, 2681–2689.
- (38) Liu, Y., and Gray, N. S. (2006) Rational design of inhibitors that bind to inactive kinase conformations. *Nat. Chem. Biol.* 2, 358–364.
- (39) Jänne, P. A., Gray, N., and Settleman, J. (2009) Factors underlying sensitivity of cancers to small-molecule kinase inhibitors. *Nat. Rev. Drug Discovery* 8, 709–723.
- (40) Nacro, K., Jeyaraj, D. A., Chennamaneni, L. R. (A*STAR, Singapore) Bicyclic Heteroaryl Derivatives as Mnk1 and Mnk2 modulators and uses thereof. International Patent WO 2013/147711 A1, October 03, 2013.
- (41) Tereshko, V., Teplova, M., Brunzelle, J., Watterson, D. M., and Egli, M. (2001) Crystal structures of the catalytic domain of human protein kinase associated with apoptosis and tumor suppression. *Nat. Struct. Biol.* 8, 899–907.
- (42) Cheek, S., Zhang, H., and Grishin, N. V. (2002) Sequence and structure classification of kinases. *J. Mol. Biol.* 320, 855–881.
- (43) Sali, A., and Blundell, T. L. (1993) Comparative protein modelling by satisfaction of spatial restraints. *J. Mol. Biol.* 234, 779–815.
- (44) Case, D., Pearlman, D. A., Caldwell, J. W.; et al. *Amber 11*, University of California: San Francisco.
- (45) Duan, Y., et al. (2003) Pointcharge force field for molecular mechanics simulations of proteins based on condensed-phase quantum mechanical calculations. *J. Comput. Chem.* 24, 1999–2012.
- (46) Wang, J., Wolf, R. M., Caldwell, J. W., Kollman, P. A., and Case, D. A. (2004) Development and testing of a general amber force field. *J. Comput. Chem.* 25, 1157–1174.
- (47) Jorgensen, W. L., Chandrasekhar, J., Madura, J. D., Impey, R. W., and Klein, M. L. (1983) Comparison of simple potential functions for simulating liquid water. *J. Chem. Phys.* 79, 926–935.
- (48) Darden, T., York, D., and Pedersen, L. (1993) Particle mesh Ewald: An $N \log(N)$ method for Ewald sums in large systems. *J. Chem. Phys.* 98, 10089–10092.
- (49) Miyamoto, S., and Kollman, P. A. (1992) Settle: An analytical version of the SHAKE and RATTLE algorithm for rigid water models. *J. Comput. Chem.* 13, 952–962.
- (50) Feig, M., Karanikolas, J., and Brooks, C. L. (2004) MMTSB tool set: enhanced sampling and multiscale modeling methods for applications in structural biology. *J. Mol. Graph. Model.* 22, 377–395.
- (51) Humphrey, W., Dalke, A., and Schulten, K. (1996) VMD—visual molecular dynamics. *J. Mol. Graph.* 14, 33–38.
- (52) De Lano, W. (2002) *The PyMOL Molecular Graphics System*, De Lano Scientific, San Carlos CA, USA.
- (53) Kaminski, G. A., Friesner, R. A., Tirado-Rives, J., and Jorgensen, W. L. (2001) Evaluation and reparametrization of the OPLS-AA force field for proteins via comparison with accurate quantum chemical calculations on peptides. *J. Phys. Chem. B* 105, 6474–6487.
- (54) *Schrodinger*, version 9.0, Schrödinger, LLC, New York, 2009.
- (55) Friesner, R. A., Banks, J. L., Murphy, R. B., Halgren, T. A., Klicic, J. J., Daniel, T., Repasky, M. P., Knoll, E. H., Shelley, M., and Perry, J. K. (2004) Glide: a new approach for rapid, accurate docking and scoring. I. Method and assessment of docking accuracy. *J. Med. Chem.* 47, 1739–1749.
- (56) Hou, T. J., Wang, J., Li, Y. Y., and Wang, W. (2011) Assessing the performance of the molecular mechanics/Poisson Boltzmann surface area and molecular mechanics/generalized Born surface area methods. II. The accuracy of ranking poses generated from docking. *J. Comput. Chem.* 32, 866–877.
- (57) Homeyer, N., and Gohlke, H. (2012) Free Energy Calculations by the Molecular Mechanics Poisson-Boltzmann Surface Area Method. *Mol. Inf.* 31, 114–122.

- (58) Wang, J. M., Hou, T. J., and Xu, X. J. (2006) Recent advances in free energy calculations with a combination of molecular mechanics and continuum models. *Curr. Comput.-Aided Drug Des.* 2, 287–306.
- (59) Guimarães, C. R., et al. (2011) Understanding the Impact of the P-loop Conformation on Kinase Selectivity. *J. Chem. Inf. Model.* 5, 1199–1204.
- (60) Patel, R. Y., and Doerksen, R. J. (2010) Protein kinase–inhibitor database: Structural variability of and inhibitor interactions with the protein kinase P-loop. *J. Proteome Res.* 9, 4433–4442.
- (61) Yibing, S., Anton, A., Eric, T. K., Albert, C. P., and David, E. S. (2013) Transitions to Catalytically Inactive Conformations in EGFR Kinase. *Proc. Natl. Acad. Sci. U.S.A.* 110, 7270–7272.
- (62) Albert, C. P., Thomas, M. W., Yibing, S., Daniele, P. S., and David, E. S. (2014) Assessing the Accuracy of Two Enhanced Sampling Methods Using EGFR Kinase Transition Pathways: The Influence of Collective Variable Choice. *J. Chem. Theory Comput.* 10, 2860–2865.
- (63) Woods, C. J., Malaisree, M., Long, B. J. O., McIntosh-Smith, S. N., and Mulholland, A. J. (2013) Analysis and assay of oseltamivir-resistant mutants of influenza neuraminidase via direct observation of drug unbinding and rebinding in simulation. *Biochemistry* 52, 8150–8164.